JTTEE5 12:101-111

In-Flight Characteristics of Plasma Sprayed Alumina Particles: Measurements, Modeling, and Comparison

M.P. Planche, R. Bolot, and C. Coddet

(Submitted 5 June 2001; in revised form 1 August 2001)

The key phenomena controlling the properties of sprayed coatings are the heat and momentum transfer between the plasma jet and the injected particles. Modern on-line particle monitoring systems provide an efficient tool to measure in-flight particle characteristics in such a way that factors that could affect the coating quality can be identified during the spray process. In this work, the optical sensing device, DPV-2000 from Tecnar, was used for monitoring the velocity, temperature, and diameter of in-flight particles during the spraying of alumina with a Sulzer-Metco F4 plasma torch. Evolution of particle velocity, temperature, diameter, and trajectory showed well-marked trends. Relationships between the position of the in-flight particles into the jet and their characteristics were pointed out, thus delivering valuable information about their thermal treatment. Moreover, a numerical model was developed and predictions were compared with experimental results. A good agreement on particle characteristics was found between the two different approaches.

Keywords alumina, numerical model, particle diagnostics

1. Introduction

For plasma spraying processes, particle velocity determines particle dwell time in the jet that in turn has a strong effect on particle melting or evaporation, and finally, on coating properties.[1] Therefore, production of reliable and repeatable coatings requires precise control of the spray parameters to obtain the maximum benefit of heat and momentum transfer from the plasma jet to the sprayed particles. As a consequence, different diagnostic methods have been developed in the past few years in such a way that particle characteristics could be determined and related to the physical phenomena involved. Generally, on-line measurements principally concern velocity and surface temperature of particles. Particle parameters were obtained from Laser Doppler Velocimetry (LDV) and the two-color pyrometry technique.[2-5]

In the present work, particle characteristics were measured using the optical system DPV-2000 from Tecnar (Quebec, Canada).[6,7] This system, based on the detection and analysis of particle radiation, allows the determination of the velocity, temperature, and diameter of in-flight particles, as well as their trajectory into the plasma jet. To further explore the capabilities of this system, an alumina powder was sprayed with a Sulzer-Metco F4 plasma torch (Wohlen, Switzerland), and the behavior of the corresponding particles was analyzed.

A second approach was also undertaken using numerical modeling. This approach, based on the use of the Phoenics CFD software (CHAM, London, UK), consisted of a 2D-axisymmetric free jet calculation using the k-ε model of Chen and Kim.[8] Calculations were developed for determining the temperature and velocity fields in the jet. Moreover, interactions between the plasma and the particles were calculated from 2D transport equations, thus allowing a comparison between experimental and numerical results.

The aim of this work is to compare experimental results obtained on alumina particle characteristics with results predicted using the in-house code. Finally, the modeling could be used for other ceramic materials to estimate the influence of the spray parameters before experiments and to gain a deeper insight into the process of the plasma spraying of ceramic materials.

The following paper presents the experimental set-up, the experimental and calculated particle characteristics, and a comparison between the two.

M.P. Planche, R. Bolot, and **C. Coddet,** LERMPS–UTBM, 90010 Belfort, France. Contact e-mail: marie-pierre.planche@utbm.fr.

Nomenclature

V_p	particle velocity	$m \cdot s^{-1}$
V_g	gas velocity	$m \cdot s^{-1}$
Cd	drag coefficient	
d	particle diameter	m
ρ_p	particle density	$kg \cdot m^{-3}$
ρ_∞	plasma density at T_∞	$kg \cdot m^{-3}$
ϕ	thermal flux at the particle surface	$W \cdot m^{-2}$
α	thermal exchange coefficient	$W \cdot m^{-2} \cdot K^{-1}$
μ	dynamic viscosity	$kg \cdot m^{-1} \cdot s^{-1}$
λ	thermal conductivity	$W \cdot m^{-1} \cdot K^{-1}$
Cp	specific heat	$J \cdot kg^{-1} \cdot K^{-1}$
T_∞	local temperature of the plasma	K
T_p	particle surface temperature	K
ε_p	particle surface emissivity	
σ	Stefan constant	$W \cdot m^{-2} \cdot K^{-4}$
T_0	ambient temperature	K
H	enthalpy	$J \cdot kg^{-1} \cdot K^{-1}$

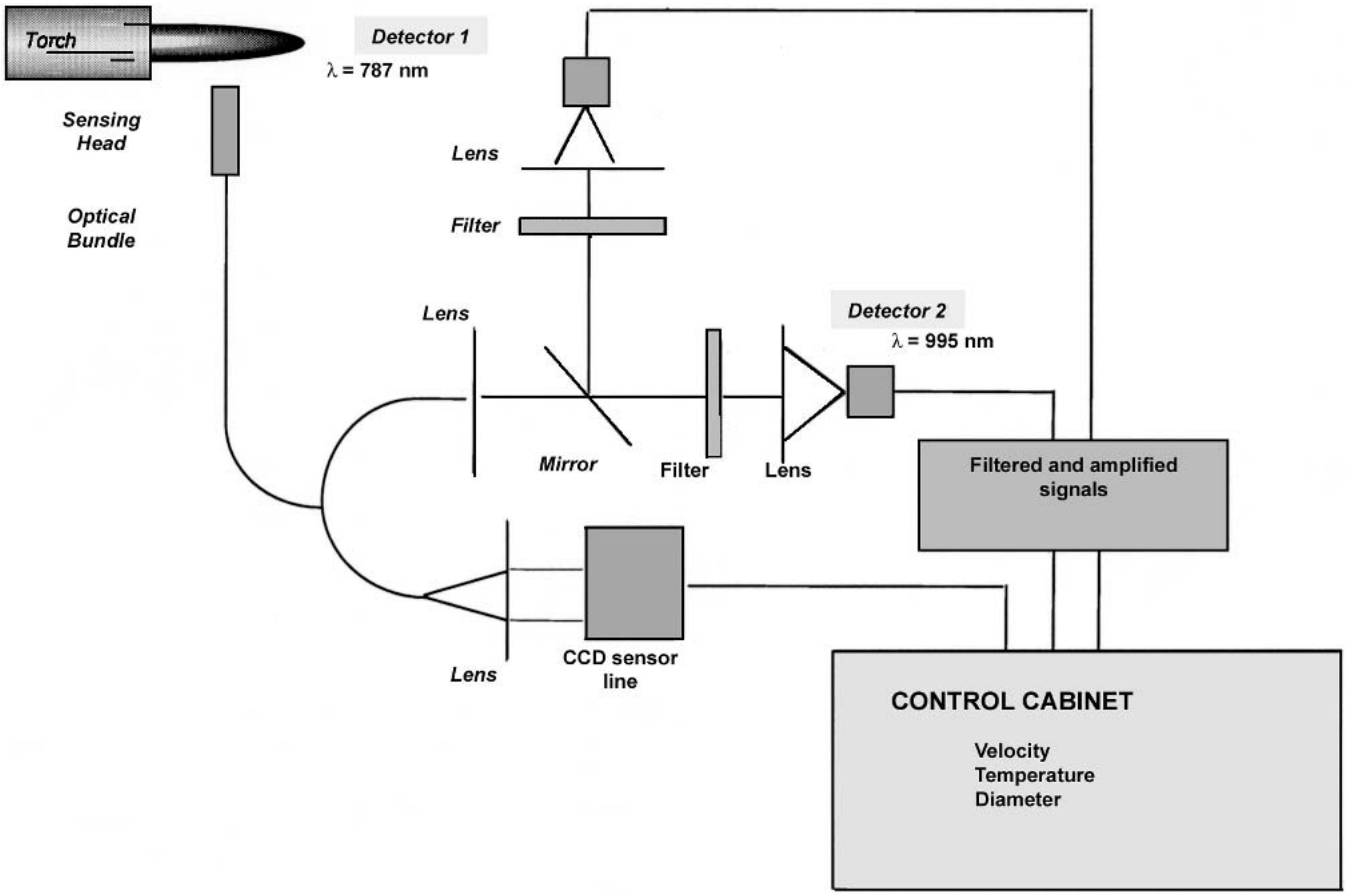

Fig. 1 Experimental set-up (DPV-2000 from Tecnar)

2. Experimental Approach

2.1 Experimental Set-Up

The schematic of the real time monitoring system is shown in Fig. 1. This system, described in detail in Ref. 6 and 7, is based on the detection of the thermal radiation emitted by a particle traveling through a measurement volume precisely localized into the plasma jet. It is comprised of a line of 50 CCD sensors used for analyzing the radial profile of the jet and of a two-slit detector connected to two pyrometers detecting individual particle emissions. Using this diagnostic method, in-flight particle characteristics (i.e., velocity, temperature, and diameter, as well as their trajectory) can be determined during the spray process.

2.1.1 Velocity Measurement. The velocity measurement is based on a time-of-flight method. In-flight particle velocity is measured by evaluating the time delay between two optical signals emitted by one particle passing through a two-slit mask. Depending on the distance between the two slits and on the definition of the collected signals, the error on the velocity measurement is around 1%.[9]

2.1.2 Temperature Measurement. The surface temperature is calculated using a two-color pyrometry technique assuming that the particle is a grey body. Two wavelengths are chosen in such a way that they correspond to a maximum particle emission and a minimum plasma emission. Notably, below a certain limit, depending on the nature of the particles, the signal cannot be detected and thus only very hot particles are observed. Due to the hypothesis and approximations that have to be made for this calculation, the accuracy of the temperature measurement is estimated at ±20 °C.[9]

2.1.3 Diameter Measurement. This parameter is deduced from the signal profile and temperature value previously determined (i.e., the amplitude of the signal is proportional to the square of the particle diameter). The diameter is computed from the absolute radiation intensity at one wavelength and the temperature of the particle. A correction factor is applied to take into account the particle material emissivity. In addition to the 3% accuracy obtained on the temperature measurement, the error on surface area must be taken into account to estimate the accuracy of the diameter measurement. That leads to almost 10% uncertainty on the diameter results.[9]

2.2 Operating Parameters

2.2.1 Plasma Conditions. The plasma torch used in this work was a Sulzer-Metco F4 gun with a 6 mm internal diameter nozzle. The gas mixture was Ar/H2 (40/14 L/min) and the arc current was about 575 A. The average voltage was 69 V for an average thermal efficiency of 57% corresponding to 22.5 kW of effective power input into the jet.

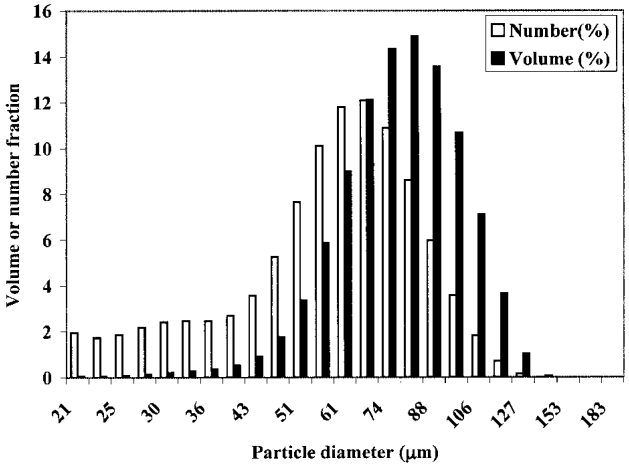

Fig. 2 Particle size distribution of the alumina powder (Amperit 740.2 from Stark)

2.2.2 Powder. The spray powder was fused and crushed alumina (Amperit 740.2 from Stark, Goslar, Germany) with a particle size distribution ranging between 45-90 μm. The particle size distribution, determined by the laser light scattering method (Laser Coulter LS130, Fullerton, CA), is given in Fig. 2 in terms of volume fraction and number fraction.

From the particle size distribution given in Fig. 2, the average particle diameter deduced was 74 μm in terms of volume fraction and 62 μm in terms of number fraction. Note that the contribution of particles smaller than 20 μm was not taken into account for the calculations because they are likely not detected, and also because their role on the coating build-up in terms of mass is probably negligible. Table 1 summarizes the differences in the size distributions in terms of volume or number fraction.

Note that even if the volume fraction of the smallest particles (<40 μm) is weak, its contribution in terms of number is significant. In contrast, the biggest particles (>100 μm) can be neglected in terms of number even if it is not the case in terms of volume.

2.3 Particle Detection

2.3.1 Particle Injection. Particles were injected at 5 mm from the exit of the torch nozzle with an injector of 1.8 mm in diameter, orthogonal to the jet axis, and with the orifice placed at 9 mm from the nozzle axis. The Ar carrier gas flow rate was adjusted at 3.1 L/min in such a way that most particles passed through the plasma jet. The powder feed rate was fixed at 6.5 g/min to obtain a good particle detection rate.

2.3.2 Location of the Measurement Volumes. The reference position (X = 0, Y = 0, Z = 0) corresponds to the origin of the plasma jet axis at the nozzle exit. A description of the coordinate system is given in Fig. 3(a).

The recordings were made at different axial (Z) distances from the nozzle exit (i.e., 60, 80, 100, and 120 mm). For each stand-off distance Z, a set of experiments was performed at different transverse locations Y, in the powder injection plane to obtain information about the particle distribution in the plasma flow. The displacement of the optical head in the Y direction was done with a step of 4 mm until the particle flux was significantly

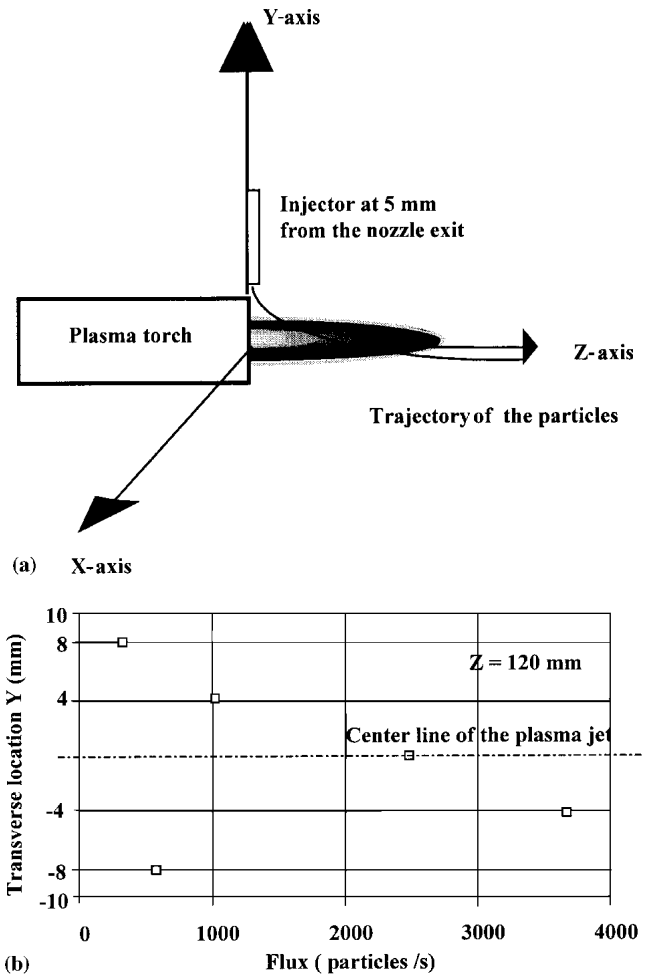

Fig. 3 **(a)** Location of the measurement volumes in the jet; **(b)** flux of particles vs the transverse locations Y at 120 mm from the nozzle exit

Table 1 Distribution of Particles Between 3 Ranges of Sizes in Terms of Volume and Number Fractions (From Laser Light Scattering Measurement)

Size	Volume Fraction	Number Fraction
from 20 to 40 μm	1.7%	17.9%
from 40 to 100 μm	86.4%	79.5%
>100 μm	11.8%	2.6%

low. Figure 3(b) gives this particle flux corresponding to the number of detected particles per second crossing the measurement volume, in function of the transverse location Y at 120 mm from the nozzle exit.

2.3.3 Recording Conditions. Data were collected with a 30 MHz sampling rate, which is high enough to get a good definition of the light signals, and were immediately processed and stored. During the spray process, the three characteristics of each particle passing through the measurement volume of the optical sensor were simultaneously determined by the DPV system.

The number of particles traveling at different locations in the plasma jet is counted, and thus, particle characteristics histograms can be plotted. Then information about the particle veloc-

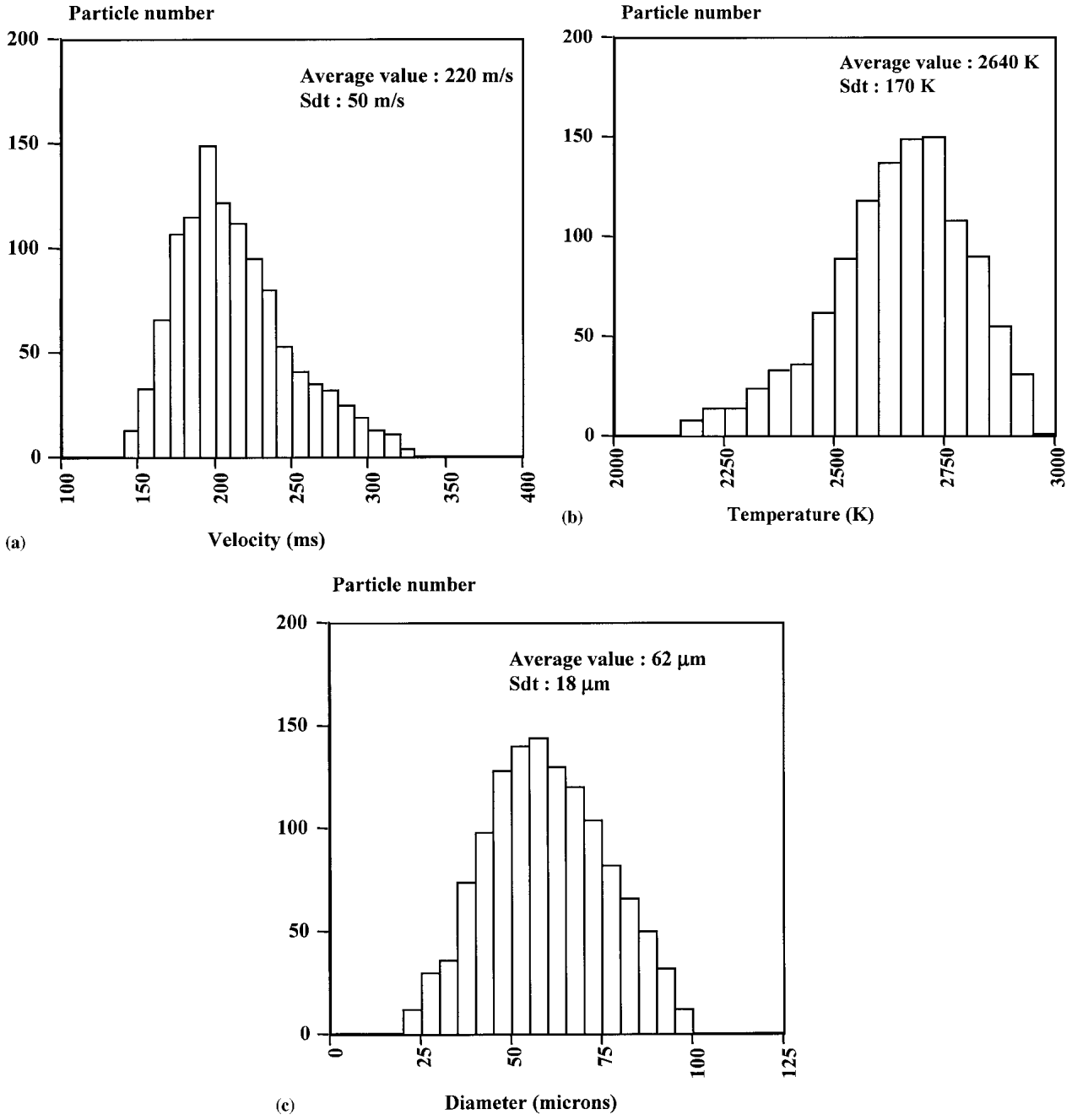

Fig. 4 **(a)**: Particle velocities histogram at Z = 120 mm from the nozzle exit on the centerline on the jet, at Y = −4 mm; **(b)** particle temperatures histogram at Z = 120 mm from the nozzle exit on the centerline on the jet, at Y = −4 mm; **(c)** particle diameters histogram at Z = 120 mm from the nozzle exit on the centerline on the jet, at Y = −4 mm

ity, temperature, and diameter distributions, as well as the position of the particle jet, are continuously updated by the computer to provide data that can be seen on the computer screen. Figure 4(a) presents an example of a particle velocities histogram obtained at Z = 120 mm from the nozzle exit and on the centerline of the particle jet (which is not the plasma jet axis).

From those statistical results, the mean particle characteristics (average values) and the standard deviation (sdt values) were calculated.

For the case presented in Fig. 4(a), the average value is about 220 m/s with a standard deviation of about 50 m/s. Similar histograms were plotted for particle temperatures and diameters (Fig. 4b and c, respectively).

The mean velocity and its standard deviation for the 120 mm stand-off distance are presented in Fig. 5, whereas the same is done for surface temperature in Fig. 6. Both were calculated from the histograms recorded for each location of the measurement volume. For each location, the acquisition time was adjusted in such a way that more than 1000 particles were recorded in the acquisition file.

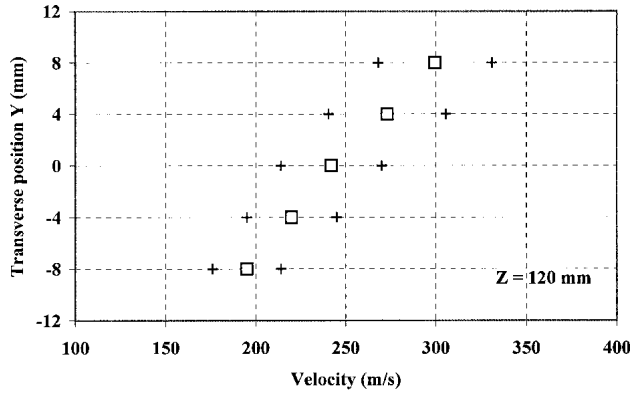

Fig. 5 Particle velocities vs their transverse location Y at Z = 120 mm

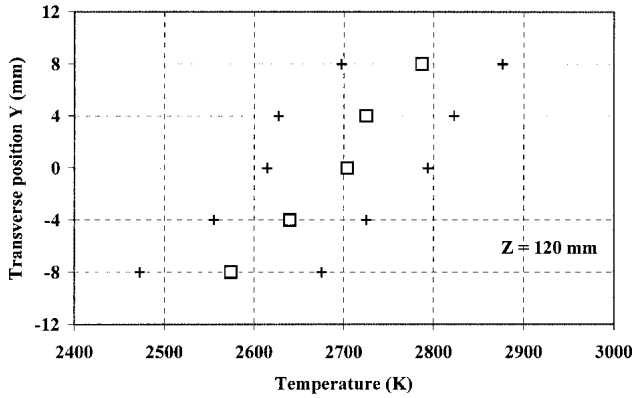

Fig. 6 Particle temperatures vs their transverse location Y at Z = 120 mm

Concerning the evolution of particle velocities, a decrease of this characteristic is observed from 300-200 m/s, when the locations of the measurement volume cross below the plasma jet axis. The evolution of the particle temperatures (Fig. 6) is similar to that of velocities, with a variation of ± 200 K on the extreme locations measured. In relation to these evolutions, the histogram of the particle diameters shown in Fig. 4(c) and obtained for a location under the plasma jet axis (Y = −4 mm) is compared with that obtained at the location Y = +4 mm above the plasma jet axis (Fig. 7). Even if the standard deviation deduced from these two histograms is large and almost the same (18 μm), some differences can be noted on the average values that increase from 51-62 μm when the measurement volume crosses below the plasma jet axis. Note that the diameter value was adjusted on the number deduced from the numerical distribution instead of the volumetric distribution. Due to the method used for the detection of the particles, this assumption corresponds much better to the real detection where the number fraction is the key parameter for the estimation of the detection rate. Indeed, some of the particles could not be taken into account due to their small size or their low emission rate.

It can then be concluded that the particle velocities and temperatures are higher when the diameters are smaller, corresponding with a location above the jet axis. Then the smallest particles, which are preferably localized over the plasma jet axis, have a greater velocity due to their smaller size. The biggest particles

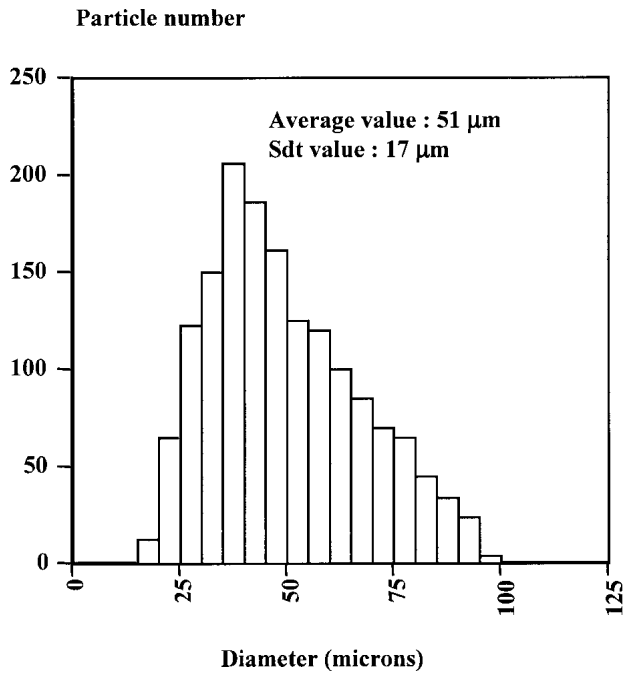

Fig. 7 Particle diameters histogram at Z = 120 mm from the nozzle exit on the centerline on the jet, at Y = +4 mm

under the plasma jet axis experience lower velocities even if they penetrate deeper into the plasma flow due to their greater momentum.

3. Numerical Approach

3.1 Presentation of the Numerical Model

Modeling was performed in two steps: the plasma jet and then the transport of particles in this plasma jet were considered. The loading effect was neglected; therefore, the calculations were performed separately.

3.1.1 Plasma Jet Modeling. A 2D model was used with the following main assumptions:

- axi-symmetric flow
- steady state flow
- plasma in local thermodynamic equilibrium (LTE) and optically thin

The effect of turbulence was taken into account by using the Chen-Kim k-ε model of turbulence,[8,10] which applies better for round jets than other k-ε models. It uses an additional source term to the ε equation and different values of the empirical constants.

The properties of the plasma and of the surrounding air were first determined using an in-house code.[11] In this code, a Gibbs free energy minimization method is used to determine the chemical equilibrium composition of each gas mixture as a function of temperature. Thermodynamic and transport properties are then deduced.

The mixing of the plasma with the surrounding air was described using an additional conservation equation for the mass fraction of Ar/H_2. By doing so, the cooling effect due to the cold

air entrainment is taken into account. However, the present model is not able to take a possible demixing of Ar and H_2 (or N_2 and O_2) into account. Nevertheless, this effect is expected to be negligible in view of the turbulent nature of the mixing process. Finally, a value of 0.7 was retained for the turbulent Schmidt number and the turbulent Prandtl number.

Velocity and enthalpy profiles were imposed at the nozzle exit following

$$v(r)/v_{cl} = (h(r) - h_w)/(h_{cl} - h_w) = (1 - (r/R)^3)$$

in which the enthalpy at the wall h_w was set for a corresponding temperature of 700 K and the centerline values of the velocity v_{cl} and enthalpy h_{cl} were determined (using an iterative method) in such a way that the plasma gas flow rate and the net power input were conserved.[11] The range of velocity in the near nozzle exit region is about 2000 m/s for a temperature higher than 12 kK.

The commercial PHOENICS code was used for the resolution of the governing equations. It is based on a finite volume approach in which the SIMPLEST algorithm is used for the discretization. Moreover, the compressibility effect was taken into account.

3.1.2 Particles. Plasma/particle interactions were calculated using an in-house code in which heat transfer inside individual particles is taken into account and is coupled to the transport equation of particles in the jet.[11] The main assumptions were:

- spherical particles that do not interact
- loading effect neglected

Finally, plasma/particle interactions were represented following:

$$\frac{d\vec{V}_p}{dt} = Cd \cdot \frac{3}{4d} \cdot \frac{\rho_\infty}{\rho_p} \cdot \left\| \vec{V}_g - \vec{V}_p \right\| \cdot (\vec{V}_g - \vec{V}_p)$$

and

$$\phi = \alpha \cdot (T_\infty - T_P) - \varepsilon_P \cdot \sigma \cdot (T_P^4 - T_0^4)$$

where the drag coefficient and the Nusselt number were calculated respectively by:

$$Cd = \frac{24}{\mathrm{Re}} \cdot \left(\frac{\overline{\rho}}{\rho_\infty} + 0{,}15 \cdot \mathrm{Re}^{0{,}687} \right) \cdot F_k^{0{,}45}$$

and

$$Nu = \frac{\alpha \cdot d}{\overline{\lambda}} = \left(2 + 0{,}6 \cdot \frac{\rho_\infty}{\overline{\rho}} \cdot \mathrm{Re}^{0{,}5} \cdot \mathrm{Pr}^{0{,}33} \right) \cdot F_k \cdot F_v$$

In these correlations, mean integrated properties between the particle surface temperature and the plasma temperature were used to determine the Reynolds and Prandtl numbers following:

$$\mathrm{Re} = \frac{\overline{\rho} \cdot |\vec{V}_g - \vec{V}_p| \cdot d}{\overline{\mu}}$$

and

$$\mathrm{Pr} = \frac{\overline{\mu} \cdot \overline{C}_p}{\overline{\lambda}}$$

The contribution of thermal radiation in the previous energy equation is small and could have been neglected.

The $\overline{\rho}/\rho_\infty$ ratio occurring in the expressions of the drag coefficient and of the Nusselt number represents the effect of variable properties in the boundary layer around the particles. It was established on the basis of theoretical considerations and has the same overall effects as corrections suggested by Huang et al.[12] for an argon plasma jet, in the sense that it increases the drag coefficient and reduces the Nusselt number somewhat similarly.

The F_K coefficient represents the Knudsen effect that was calculated using the Huang et al.[12] formula and tends to decrease thermal and dynamic exchanges. For this coefficient, an iterative method was used to determine the temperature jump at the surface of the particle. The F_V coefficient represents the vaporization effect that was calculated according to Borgianni et al.[13] or Johnston[14]correlations. Concerning the enthalpy of the decomposition products of alumina, Chase et al.[15] tables were used for thermodynamic properties of individual species and were extrapolated for temperatures above 6000 K assuming a constant specific heat. Chemical equilibrium was assumed to determine the alumina vapor composition. Nevertheless, in the present case (i.e., for refractory materials), only small particles having diameters less than 20 μm were found to be significantly affected by the vaporization effect, so that it could have been neglected given the mean particle size used in this work.

The effect of internal heat conduction was taken into account in terms of enthalpy, instead of temperature with the method described in Ref. 11 for the propagation of the front of fusion inside the particle. Moreover, a fully implicit scheme was used for time discretization.

$$\rho \frac{\partial H}{\partial t} = \frac{1}{r^2} \frac{\partial}{\partial r} \left(\lambda r^2 \frac{\partial T}{\partial r} \right)$$

Other properties of alumina were assumed to be identical to those used by Vardelle[16]

3.1.3 Powder Injection. Recent studies of particle transport within the powder injector[17,18] have shown that the particle mean injection velocity is nearly the same no matter the particle size used, and also that the dispersion in the injection velocity is the highest for the smallest particles.

In the current study, in view of the injector design (straight and short), the mean injection velocity of particles can be estimated from the acceleration of a particle of mean size along the injector (the length of which was 25 mm). In other words, it was expected that the effect of collisions tends to average the injection velocity of particles without significantly changing the overall particle momentum.

Finally, a mean injection velocity of 8 m/s was retained with a maximum deviation of ±5 m/s around this mean value.

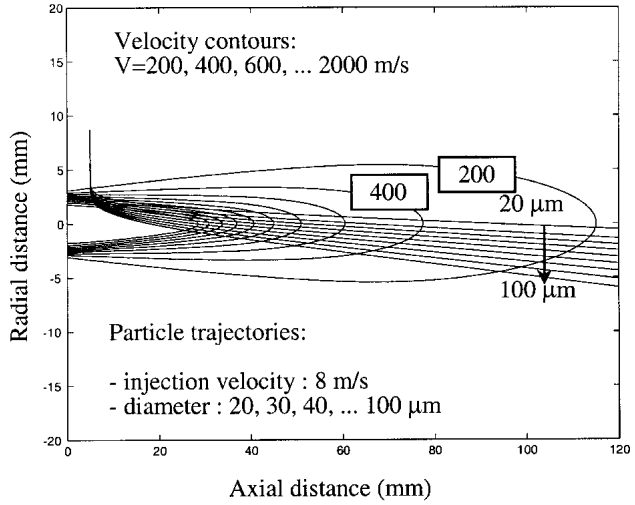

Fig. 8 Calculated velocity contours and trajectories of alumina particles of different sizes (injection velocity 8 m/s)

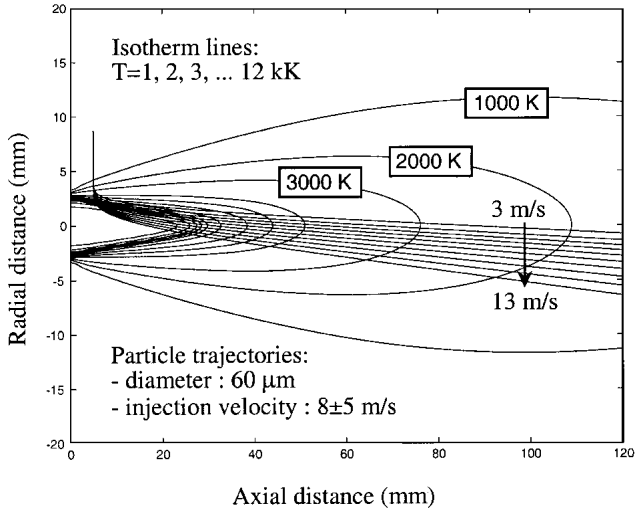

Fig. 9 Calculated isotherms and trajectories of 60 μm diameter alumina particles (injection velocity 8 ± 5 m/s)

3.2 Flow Field and Trajectories

Figure 8 presents velocity contours of the plasma jet and trajectories of different size particles injected in the plasma at 8 m/s. It can be observed that the smaller the particle, the less it penetrates within the potential core of the jet. For a stand-off distance of 120 mm, a 20 μm particle has just reached the jet axis, whereas an 80 μm particle is about 5 mm below considering the same injection velocity.

Figure 9 presents isotherms within the plasma jet and trajectories of 60 μm particles injected with an initial velocity of 8 ± 5 m/s. The axial length of isotherms is about 110 mm for the 2kK one and 50 mm for the 4kK one. Thus, it can be expected that, depending on its injection velocity, a 60 μm particle should be observed at different positions within the jet.

Figure 10 presents the computed particle velocities versus their diameter at the stand-off distance of 120 mm. The injection velocity of each class size was 8 ± 5 m/s. It can be observed that the larger the particle, the lower the mean velocity. The velocity of 60 μm particles is about 230 m/s in the present case, whereas only the smallest particles (< 40 μm) reach velocities higher than 300 m/s. The dispersion in the particle velocity is also smallest for the biggest particles. Moreover, the dispersion in the injection velocity of the largest particles was probably overestimated.

Table 2 Localization of the "Center" of Spray Jet in the Plasma Plume

Stand-off Distance Z, mm	Transverse Position Y, mm
60	0
80	−1
100	−3
120	−4

Figure 11 presents the particle surface temperature versus their diameter for the same stand-off distance of 120 mm. A tendency similar to that of velocities was observed—the smaller the particle, the higher the temperature. Particular attention must be paid to the fact that large particles (>70 μm) are likely to be unmolten according to the calculations; the maximum surface temperature being lower than the melting temperature. The critical particle size is about 70 μm, since for this diameter the core and the surface temperatures are almost identical and close to the melting temperature.

In the case of 50 μm particles, the front of fusion reaches the particle center at an axial distance of about 70 mm from the nozzle exit, as can be observed in Fig. 12. Of course, the smaller the particle, the faster it is fully molten. Thus, all 30 μm particles are fully molten at a distance of 50 mm from the nozzle exit.

In view of these results, the same tendency is observed for velocities and temperatures. Figure 13, in which the particle temperature was plotted versus the particle velocity, confirms this observation that all the particles having high velocities also have high temperatures. On the contrary, low velocity particles have a low surface temperature. In particular, the maximum temperature of particles with velocities lower than 200 m/s is the melting temperature, and all the particles having velocities lower than 150 m/s have a surface temperature under the melting point of alumina. This element can explain why the DPV system did not detect any low velocity or large diameter particles. Due to the change in the alumina emissivity at the melting temperature (0.9 for the liquid phase and 0.3 for the solid material),[16] the DPV does not detect solid particles.

As a first consequence, the DPV did not detect low velocity particles since they are probably unmolten. This fact is confirmed by temperature measurements; the DPV system did not detect particles with temperatures lower than the melting point.

4. Comparison Between Experimental and Numerical Approaches

4.1 Localization of the Mean Trajectory in the Particle Jet

The comparison between experimental and numerical results was done for the transverse locations; Y corresponding to the

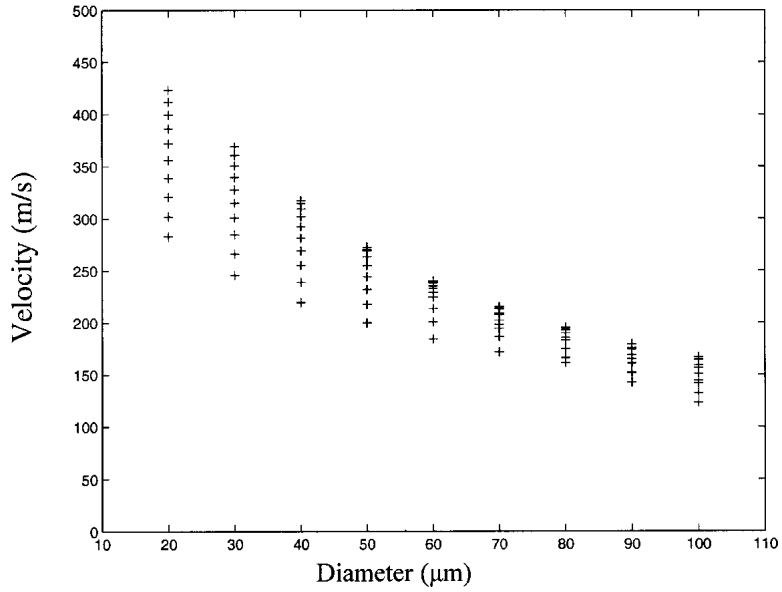

Fig. 10 Calculated alumina particles velocity vs their diameter for a stand-off distance of 120 mm

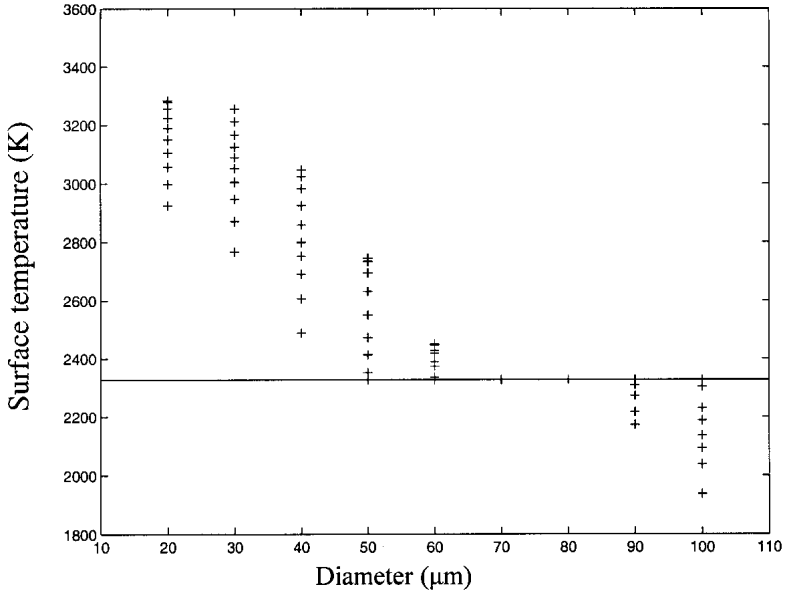

Fig. 11 Calculated alumina particles temperature vs their diameter for a stand-off distance of 120 mm

maximum particle flow rate at different axial distances Z from the nozzle exit.

Concerning the experimental results, the distance Z = 60 mm corresponds to the shortest experimental distance it was possible to test. Below this distance, plasma radiation is too high in comparison to particle radiation, thus leading to a very low particle detection rate. Due to the re-emission of the plasma radiation by the particles, calculation of particle diameter, as well as particle temperature, is affected by broadening phenomena involving an increase in the error for the measured parameters. According to the experimental results, the mean location of the detected particle maximum flux is presented in Table 2.

Considering the modeling, the particles that have a temperature less than the melting temperature are not taken into account in this comparison. According to Fig. 11, these particles have a diameter larger than 70 μm. So, the comparison was made on particles whose size is between 20-70 μm. Then, by varying the particle injection velocity between 3-13 m/s, an average value and a standard deviation were deduced from particles passing through the measurement volume (i.e., $Y = -4$ mm $\pm$ 2 mm at the Z = 120 mm distance from the nozzle exit).

The figures presented in the following section correspond to the mean velocity and temperature values, either experimental or modeled.

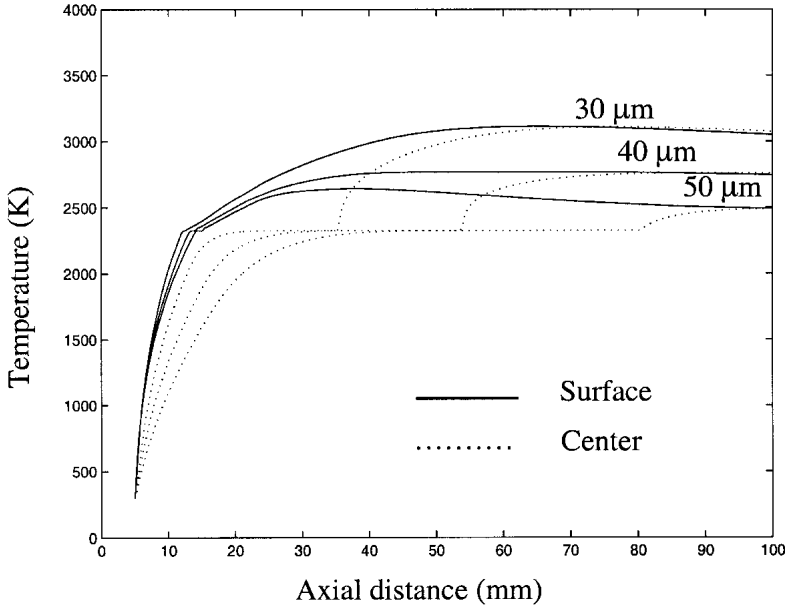

Fig. 12 Calculated surface and core temperatures of alumina particles of different sizes vs stand-off distance (injection velocity: 8 m/s; particle diameter: 30, 40, 50 μm)

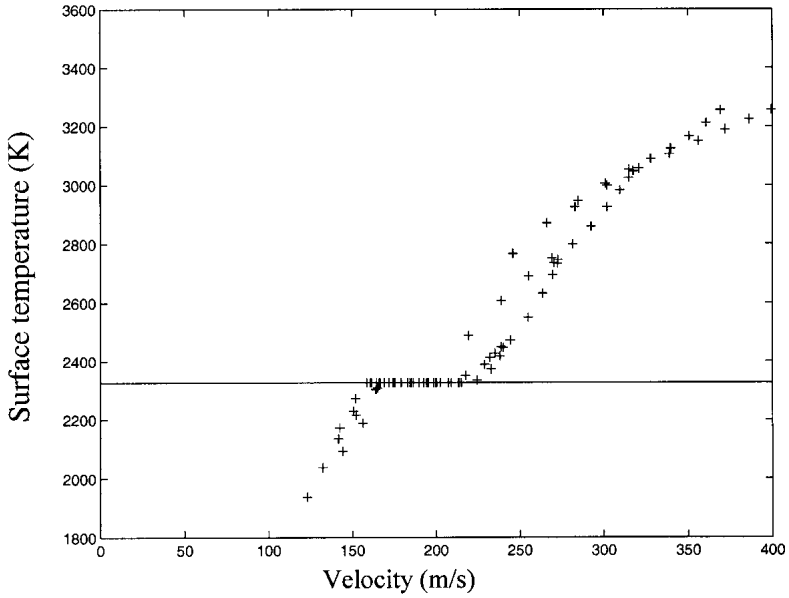

Fig. 13 Calculated alumina particles temperature vs particles velocity at Z = 120 mm from the nozzle exit

4.2 Comparison for Velocity and Temperature Results Versus the Stand-Off Distance Z Taken From the Nozzle Exit

As can be noted in Fig. 14, velocities obtained experimentally are consistent with those predicted by numerical calculation. However, the discrepancy between both results seems more important in the case of the shortest distance Z from the nozzle exit; this should probably be attributed to the difficulty of particle detection at this distance.

Concerning temperature values (Fig. 15), differences observed between experimental and numerical approaches are less than 100 K, regardless of axial distance and standard deviations.

According to these results and with a standard deviation being around 10%, whatever the particle characteristics, it can be estimated that a good agreement exists between the two approaches for velocity as well as for temperature.

4.3 Comparison for Velocity Results in the Transverse Position Y From the Jet Axis

The comparison presented in Fig. 16 was made for the Y positions below the jet axis (i.e., for the particles crossing the jet axis). Indeed, some particles were experimentally observed above the jet axis. The corresponding trajectories do not exist in the case of the model, which did not take into account the fluc-

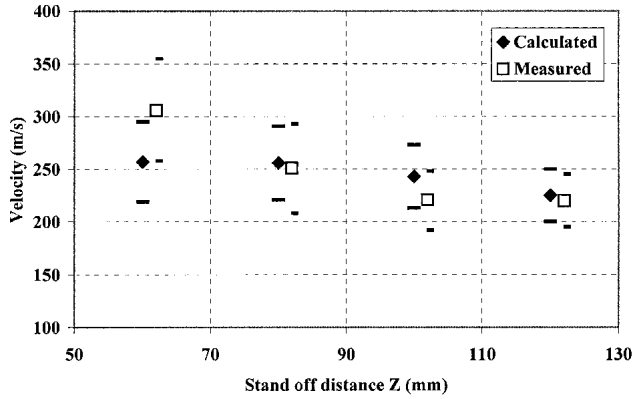

Fig. 14 Comparison between measured and calculated mean velocities of alumina particles on the centerline of the jet

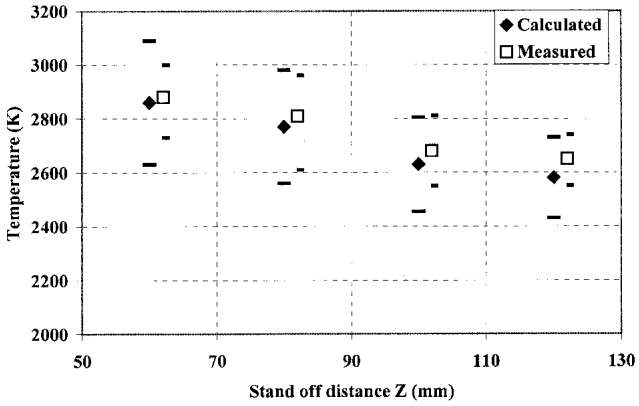

Fig. 15 Comparison between measured and calculated mean temperatures of alumina particles on the centerline of the jet

tuations of the plasma jet (steady state assumption). However, the number of particles detected at $Y > 0$ was much smaller than the number of particles observed at $Y < 0$, so that the model was considered to be sufficiently representative.

Again, a good agreement is observed between experimental and numerical results. First, the particles detected on the jet axis ($Y = 0$) have a higher velocity than particles that cross the jet ($Y = -8$ mm). The main reason is that the mean particle size at $Y = 0$ is smaller than at $Y = -8$ mm, so that they have a higher velocity. Second, the standard deviation is higher at $Y = 0$ than at $Y = -8$ mm. This is in accordance with the mean particle size since the largest particles have a more homogeneous velocity than the smallest ones. This could be explained by the large distribution of the particles into the jet at $Z = 120$ mm.

5. Conclusion

The main objective of this work was to compare experimental results and numerical modeling to improve the understanding of interactions between plasma and particles. The calculated temperatures and velocities of the particles were compared with the measured values obtained with the DPV diagnostic system. Some conclusions can be drawn at this stage.

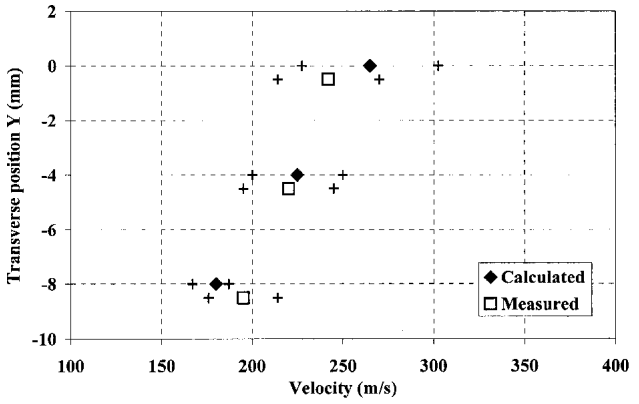

Fig. 16 Comparison between measured and calculated velocities for the stand-off distance $Z = 120$ mm

Modeling and experimental results of particle characteristics have shown that velocities and temperatures are highest when the trajectory of the particles is above the jet axis, which corresponds therefore to the smallest particle diameters. The calculated particle velocities and temperatures are in good agreement with the experimental results; the discrepancies are less than 10% between both approaches.

The particles are experimentally detected within a large radial position in the plasma jet in comparison to the modeling, indicating a marked dispersion of the particles in the flow as a result of the high plasma fluctuations and turbulence, which is not theoretically taken into account (steady state assumption). Then the mean particle trajectory has been experimentally determined and shows that the majority of the particles pass through the hottest regions of the plasma. The influence of the injection velocity and diameter of the particles is clearly explained by the model to find satisfactory parameters.

For the ceramic powder used in this work, the model points out the possibility of having partly molten or unmelted particles; that explains the experimental evolution obtained on experimental particle characteristics far from the nozzle exit.

For a given particle size, the model indicates that the particle velocity and temperature reach a maximum at $Y = -3$ mm for the $Z = 120$ mm stand-off distance. This criterion could be used to optimize the carrier gas flow rate so that the particles are detected.

References

1. J. Fincke, W. Swank, and D. Haggard: "Plasma Spraying of Alumina: Plasma and Particle Flow Fields," *Plasma Chem. Plasma Processing*, 1993, *13*(4), pp. 579-99.
2. M. Vardelle, A. Vardelle, A.C. Leger, and P. Fauchais: "Dynamics of Splat Formation and Solidification in Thermal Spraying Processes" in *Thermal Spray Industrial Applications*, C.C. Berndt and S. Sampath, ed., ASM International, Materials Park, OH, 1994, pp. 555-62.
3. R. Knight, R.W. Smith, and Z. Xiao: "Particle Velocity Measurements in HVOF and APS Systems" in *Thermal Spray Industrial Applications*, C.C. Berndt and S. Sampath, ed., ASM International, Materials Park, OH, 1994, pp. 331-36.
4. P. Gougeon, C. Moreau, and F. Richard: "On-Line Control of Plasma Sprayed Particles in the Aerospace Industry" in *Advances in Thermal Spray Science and Technology*, C.C. Berndt and S. Sampath, ed., ASM International, Materials Park, OH, 1995, pp. 149-55.
5. T. Lehtinen, J. Knuuttila, J. Vattulainen, T. Mantyla, and R. Hernberg: "Correlations Between In-Flight Particle Concentrations and Coating Properties in Atmospheric Plasma Spraying Alumina" in *Thermal*

Spray: Practical Solutions for Engineering Problems, C.C. Berndt, ed., ASM International, Materials Park, OH, 1996, pp. 525-30.
6. L. Leblanc, P. Gougeon, and C. Moreau: "Investigation of the Long Term Stability of Plasma Spraying by Monitoring Characteristics of the Sprayed Particles" in *Thermal Spray: A United Forum for Scientific and Technological Advances*, C.C. Berndt, ed., ASM International, Materials Park, OH, 1997, pp. 567-75.
7. C. Moreau: "Towards Better Control of Thermal Spray Processes" in *Thermal Spray: Meeting the Challenges of the 21st Century*, C. Coddet, ed., ASM International, Materials Park, OH, 1998, pp. 1681-93.
8. Y.S. Chen and S.W. Kim: "Computation of Turbulent Flows Using an Extended k-ε Turbulence Closure Model," NASA Report CR-179204, 1987.
9. C. Moreau, P. Gougeon, M. Lamontágne, V. Lacasse, G. Vandreuil, P. Cielo: "On-Line Control of the Plasma Spraying Process by Monitoring the Temperature, Velocity and Trajectory of In-Flight Particles" in *Proc. of 7th National Thermal Spray Conference*, Boston, MA 1994, pp. 431-37.
10. R. Bolot, M. Imbert, and C. Coddet: "On the Use of a Low Reynolds Extension to the Chen-Kim (k-ε) Model to Predict Thermal Exchanges in the Case of an Impinging Plasma Jet," *J. Heat and Mass Transfer*, 2001, *44*, pp. 1095-1106.
11. R. Bolot: "Modélisation des Écoulements de Plasmas d'arc Soufflé: Application à la Projection de Matériaux Pulvérulents," Ph.D. Thesis, Université de Franche-Comté, 1998 (in French).
12. P.C. Huang, J. Heberlein, and E. Pfender: "Particle Behavior in a Two Fluid Turbulent Plasma Jet," *J. Surface and Coatings Technol.*, 1995, *73*, pp. 142-51.
13. C. Borgianni, M. Capitelli, F. Cramarossa, L. Triolo, and E. Molinari: "The Behavior of Metal Oxydes Injected Into an Argon Induction Plasma," *J. Combustion and Flame*, 1969, *13*, pp. 181-94.
14. P.D. Johnston: "The Rate of Decomposition of Silica Particles in an Augmented Flame," *J. Combustion and Flame*, 1972, *18*, pp. 373-79.
15. M. Chase, C. Daves, J. Downey, D. Frurip, R. McDonald, A. Syrerud: "Janaf Thermodynamical Table," *J. Phys. Chem. Reference Data, 14* (Suppl. 1), 1985, pp. 61-67, 140.
16. A. Vardelle: "Etude Numérique des Transferts de Chaleru, de Quantité de Mouvement et de Masse Entre un Plasma d'arc à la Pression Atmosphérique et des Particules Solides," Ph.D. Thesis, Université de Limoges, 1987 (in French).
17. J.R. Fincke, W.D. Swank, and D.C. Haggard: "In-Flight Behavior of Dissimilar Co-injected Particles in the Spraying of Metal-Ceramic Functionally Graded Materials" in *Thermal Spray: A United Forum for Scientific and Technological Advances*, C.C. Berndt, ed., ASM International, Materials Park, OH, 1997, pp. 527-34.
18. M. Vardelle, A. Vardelle, P. Fauchais, B. Dussoubs, T. Roemer, R. Neiser, and M. Smith: "Influence of Injector Geometry on Particle Trajectory: Analysis of Particle Dynamics in the Injector and Plasma Jet," *Thermal Spray: Meeting the Challenges of the 21st Century*, C. Coddet, ed., ASM International, Materials Park, OH, 1998, pp. 887-984.